Simplified Computational Model of the Cervical Region for Transcutaneous Spinal Direct Current Stimulation

L. O. Fernandes[1,2(✉)], C. M. Germer[3], and P. X. de Oliveira[1]

[1] FEEC/DEEB, University of Campinas (UNICAMP), Campinas, Brazil
lofernandes@uesc.br
[2] DCET, University of Santa Cruz (UESC), Ilhéus, Brazil
[3] DEBM, University of Pernambuco (UFPE), Recife, Brazil

Abstract. Transcutaneous spinal direct current stimulation (tsDCS) is a neuromodulation technique used for the rehabilitation of spinal cord disorders and injuries. Despite its potential effect, the stimulation parameters are not well established, and the underlying effects of tsDCS on the neural mechanisms in the spinal cord remain unknown. A common approach to these problems is the use of computer models to simulate both the electric field in the targeted region and the neural response to the stimulus. Nevertheless, these models are limited, especially for tissues in the cervical region. Thus, this paper presents a model of the volume conductor for the cervical region and optimized simulations using the finite element method in the solution of the current flow problem induced by the application of tsDCS. It was possible to obtain a volume conductor model representing different tissues: skin, subcutaneous fat, muscle, trachea, esophagus, cartilage, vertebral ligaments, vertebrae, vertebral arteries, intervertebral discs, duramater, cerebrospinal fluid, white and gray matter of the spinal cord. Three meshes with different element densities were produced (low, intermediate, and high resolution). The lower density mesh showed an electric field with a mean square error between 6.21% and 2.50% in the spinal cord tissues when compared to the higher resolution mesh. Therefore, the optimization proposed reached acceptable errors and allows multiple simulations, using different setups (conductivities, current intensity, geometric and positions of electrode) with less computational cost (88 min to 17 min for runtime and 4 GB to 800 MB for local storage).

Keywords: Electric field · Spinal cord · Finite element method · Optimization

1 Introduction

Electrical stimulation has been widely employed for therapeutic purposes throughout history. Late reports (43–48 A.D.) indicate the use of electrical discharges from torpedo fish in the treatment of headache [1]. Despite the diversity of techniques for stimulation (e.g., invasive, non-invasive, electrical, magnetic, alternating, and continuous), all of them are similar in their purpose of altering the functioning of the nervous system.

J. L. B. Marques et al. (Eds.): CLAIB 2022/CBEB 2022, IFMBE Proceedings 98, pp. 266–276, 2024.
https://doi.org/10.1007/978-3-031-49401-7_26

In general, techniques using DC stimulation are safe and inexpensive, which allows for different experimental treatment options in patients with disorder of central nervous system [2–4]. While stimulation at high intensities can directly evoke neural activation via action potential (AP), low-intensity stimulation influences neural functioning without the direct generation of APs. Recently, direct current stimulation (DCS) has been employed in a noninvasive way to promote modulatory effects on spinal motor circuitries [2]. However, the effects elicited by transcutaneous spinal direct current stimulation (tsDCS) still being poorly understood [5].

A low-intensity direct current (DC) applied to the skin at a targeted region of the spinal cord induces an electric field which causes short or long-term functional changes in the neural pathways [6]. Thus, the main goal of tsDCS in the cervical region is to modulate the behavior of the local neural circuits and the spinal pathways' excitability [6–8].

Due to the nature of the electric field interaction on tissues, different results are observed depending on the dose, the region of interest, and the positioning and shape of the electrodes. Also, the conditions of inhomogeneity, anisotropy, and the geometric complexity of the tissues difficult the analytical solution to the volume conductor problem [9, 10]. Therefore, computational modeling of the electrical stimulation of the central nervous system (computational neurostimulation) is an important tool for understanding how and which spinal mechanisms are affected by the application of tsDCS, and how it can be employed to promote the desired changes.

The finite element method (FEM) is one of the main computational modeling techniques employed to predict the current flow and the electric field in different segments of the spinal cord. It allows considering the different characteristics, properties, and locations of the tissues and electrodes [6]. Thus, an important advantage of FEM is its application in problems with high geometric complexity and/or a diversity of electrical properties.

The partial differential equations (EDP) problems, like presented above, are solved by FEM, where the solution domain is discretized into several finite elements, uniform or not, connected by nodes [10]. From this breakdown, usually into tetrahedral elements for the three-dimensional model, it is possible to compute the electric field in each element. The solution can be approximated by numerical methods, considering the material property in a system of simplified equations. However, in addition to the availability of the geometric model of the volume conductor, the number of mesh elements is directly linked to the accuracy of the solution, and this requires more computational capacity (runtime, memory, and storage) to FEM solver.

Computational models of volume conductors are essential for predicting the setups needed so that the clinical target of tsDCS can be safely achieved. However, there are still few studies that use computational modeling of tsDCS application, and those are focused on the thoracic and lumbar regions of the spinal cord [11, 12], whereas few works have focused on the cervical region [13, 14]. Perhaps one of the main reasons is the complexity involved in the construction process or the lack of availability of volume conductor models of the cervical region. Despite the models provided by the ViP (Virtual Population) library being accessible and based on real segmentation of human body tissues [15, 16], they present simplifications in their composition, when

provided in their open format version, that may affect the desired simulation result in the region of interest.

The objective of this study is to present a simplified volume conductor model that would represent the human cervical region. Furthermore, we aim to evaluate how the model optimization interferes with the solution of the problem using FEM.

2 Materials and Methods

2.1 Volume Conductor Model of Cervical Region

The simplified model proposed in this study was built from anatomical data of the cervical region [16], using the geometric tool from COMSOL (v5.3, Stockholm, Sweden) and performed in a notebook computer with a 2.21 GHz Intel® Core™ i7-8750H processor, 64 GB DDR4 RAM and 512 GB NVMe storage. For this purpose, the following tissues were considered: the cervical vertebrae C2 to C7 [16–18]; the white (WM) and gray (GM) matter of the spinal cord [19]; the cerebrospinal fluid (CSF); the intervertebral discs [20]; the vertebral arteries [21]; the duramater [22]; the longitudinal, capsular, supraspinal, interspinal, and flavum ligaments [23, 24]; cartilage of the articular facet [25]; walls of the esophagus [26] and trachea [27]; musculature [16]; subcutaneous fat [16]; and skin [16].

Figure 1 shows the modeled vertebra overlayed by the anatomical C5 vertebra of the Duke V2.0.1 model from the ViP library [16] for comparison. Based on the average value of the anatomical parameters of the C2 to C7 vertebrae, a single model shows: body height of 12 mm; spinal canal width of 25 mm and depth of 17 mm; total length and width of 55 mm and 52 mm, respectively. In addition, each vertebra had both cortical and trabecular bones modeled [18], where the cortical shell thickness has an average value of 0.527 mm.

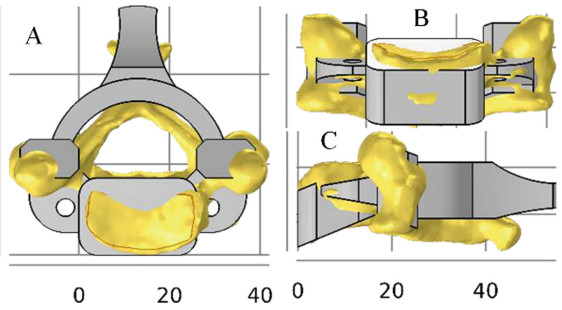

Fig. 1. Model used to represent all vertebrae in the cervical region (gray) and reference model built from real segment of C5 vertebra (yellow). Views with dimension in mm: transverse (A), anterior (B), and lateral (C).

Figure 2.A shows eight bidimensional segments of the cervical spinal cord segmented from diagrams based on Nissl images [19] and used to compose the tridimensional model of the cervical region (Fig. 2.B). The lordosis (curvature) of the cervical region was

ignored. The initial (C1) and final (C8) segments of the spinal cord have been extended beyond their intercervical limits, allowing the GM geometry to end in these regions, avoiding direct contact with the CSF.

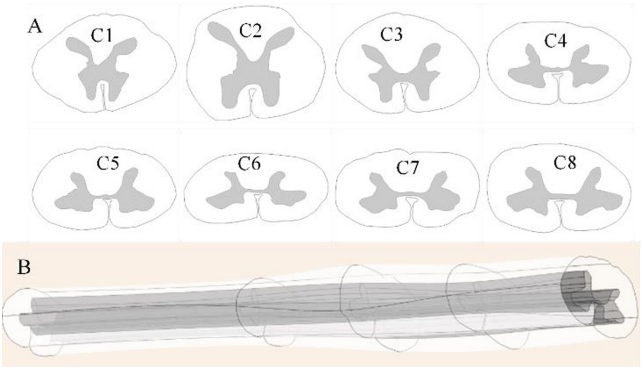

Fig. 2. A) Bidimensional segments for eight cervical sections of the spinal cord. B) Tridimensional model of the cervical region up to segment C5.

The geometric building of the remaining tissues was based on anatomical sizes (e.g., width, thickness, length, or height) or by approximation using the Duke V2.0.1 model [16]. The average value of the tissue dimensions in each segment of the cervical region was used in the individual geometry that forms the vertebra assemblies. The tissues that exhibit a large extension along the longitudinal axis, hold constant anatomical dimensions. Figure 3 shows the volume conductor model, it is composed of 13 vertebra assemblies (vertebra, disc, articular facet cartilage, flavum, and capsular ligaments) and other tissues that composes the cervical region, as presented above. In total, the geometric model had a volume of 2,953,800 mm^3 (2.96 L), with a diameter of 127 mm and height of 232 mm, presenting a total of 173 domains (geometric entities).

The standard position of the electrodes is given in the anterior (anode) and posterior (cathode) central region of the volume conductor. The electrode set (anode and cathode), with parameterizable dimension and positioning, is formed by the electrode ($49 \times 49 \times 1$ mm^3), the conductive gel/sponge ($50 \times 50 \times 2.5$ mm^3), and a representation of wire conductors (bottom edge of electrode) with a length of 1 mm and a cross-sectional area of 1 mm^2.

2.2 Mesh Parameterization

COMSOL (v5.3, Stockholm, Sweden) has five parameters for generating the FEM mesh of the geometric model: maximum element size; minimum element size; maximum element growth rate; curvature factor and resolution of narrow regions. These parameters can be filled from predefined sets (e.g., Extremely Fine, Fine, Normal, and Extremely Coarse) or individual values, uniformly or individually applied on the geometric entities and furthermore, control the mesh resolution (number of elements in the mesh).

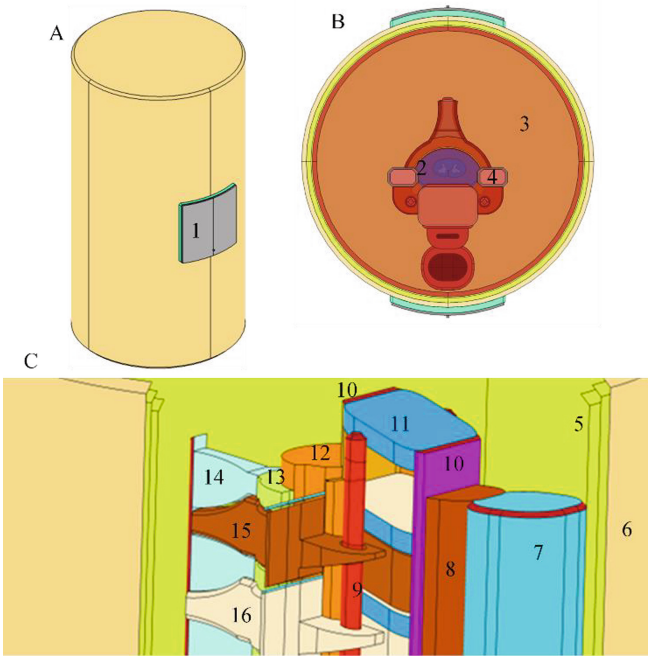

Fig. 3. Volume conductor proposed and its views with some tissues: 3D isometric (A), Transverse with tissues transparence (B), and 3D isometric with tissues details (C). The electrode (1) is placed on the anterior region. The view B shows: the spinal cord, composed by gray and white matters, and evolved by the cerebrospinal fluid (2); the articular cartilage facet and the capsular ligament (4). The vertebrae (16) are surrounded by muscle (3) and ligaments (4, 10, 13 and 14). More externally is the subcutaneous fat (5), rounded by skin (6). There are the: trachea (7), the esophagus (8), vertebral artery (9), longitudinal ligaments (10), disk (11), duramater (12), flavum ligament (13), interspinal ligament (14), trabecular bone of vertebrae (15), and the cortical shell vertebrae (16).

Additionally, COMSOL (v5.3, Stockholm, Sweden) provides different quality measures, in which the "Skewness" measure is the default and most suitable for most types of meshes. The "Skewness" is a measure of the equiangular skew and has values between 0 and 1, where 1 represents a perfectly regular element, and 0 represents an element with high or small angles (between edges). While for values under 0.01 is considered very low, the values above 0.1 are suitable for simulations. Since the accuracy of results is also associated with mesh quality, COMSOL (v5.3, Stockholm, Sweden) allows us automatically to measure, in the whole volume conductor or individual tissues, the minimum and average quality during the mesh building process.

From the geometric models, three mesh types were produced with different resolutions (Fig. 4). Mesh 1 was considered the reference for its high resolution and standard predefinition "Extremely Fine". The tissues were parameterized individually and manually for meshes 2 and 3 using the five parameters described above, attending for the minimum (> 0.01) and average (> 0.1) quality values during the mesh generation process.

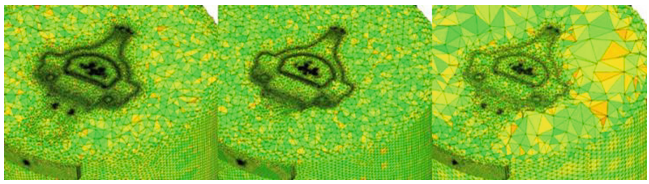

Fig. 4. Cross-section in the central region of the volume conductor showing the distribution of tetrahedral elements for high, intermediate, and low-resolution mesh (left to right). The distortion quality of each element is indicated by the tone level, green for higher and red for lower quality.

For each mesh, it is possible to observe the differences in the elements density of some tissues, indicated by the delineation pattern formed between the interfaces of the elements. In mesh 1, there is a higher density of elements per tissue when compared to meshes 2 and 3. While mesh 2 shows a density reduction in some tissues (e.g., vertebra, trachea, and esophagus), mesh 3 shows a considerable reduction in the elements density throughout the tissues when compared to mesh 1.

As shown in Table 1, mesh 3 presented the smallest processing time, the lowest number of elements, and a small distortion in the total volume. The meshes 2 and 3 maintained the Minimum Quality but slightly reduced the Average Quality in comparison with mesh 1. Even though the number of elements in mesh 2 was intermediate, the processing time was the longest.

Table 1. Processing time (single runtime) and mesh data

Mesh	Time (min)	Volume (mm3)	Elements	Minimum Quality	Average Quality
1	37	2.96×10^6	5.46×10^7	0.02	0.68
2	99	2.96×10^6	4.47×10^7	0.02	0.65
3	11	2.95×10^6	5.85×10^6	0.02	0.65

2.3 Tissue Dielectric Properties

The tsDCS electric field distribution across the neck region was described by Maxwell's equations and, considering the static regime of the phenomenon, follows the formulations of electrostatics. The stationary electric potential in the inhomogeneous conductive volume model was computed using the AC/DC Electric Currents module of the COMSOL (v5.3, Stockholm, Sweden) for solving the EDP of the current flow in the volume conductor, neglecting the neurophysiology of the nervous tissue [29]:

$$\nabla \cdot (-\sigma V) = 0 \tag{1}$$

where, V is the electric potential, σ is the electrical conductivity of volume conductor. The boundary conditions have been configured in COMSOL (v5.3, Stockholm, Sweden)

to treat all outside boundaries as electrically isolated (except by the surface of electrodes) and all internal boundaries as continuous between the interfaces. For the electrodes in bipolar configuration, the applied current was defined as cathode Ic = −2.5 mA and anode Ia = 2.5 mA. The stationary solver in the conjugate gradient configuration was used during the simulations and adjusted with a relative tolerance of 10^{-6}.

2.4 Electric Field Analysis

A tsDCS simulation was performed for each mesh, assuming the properties and configurations presented in the Sects. 2.1 and 2.2. Data analysis was performed in MATLAB (R2021a, Massachusetts, USA). The electric field was obtained at the spatial nodes of the whole volume of WM and GM tissues, and the average magnitude of the electric field E was estimated in volumetric sections of 0.5 mm. In order, to evaluate the effect of the mesh resolution on the electric field at the spinal cord, mesh 1 was taken as reference, and the electric field error of meshes 2 and 3 was estimated with the mean absolute error (MAE), the mean absolute percentage error (MAPE), and the normalized root mean square error (NRMSE).

$$MAE = (1/n)\,\Sigma\left|y_i - \hat{y}_i\right| \tag{2}$$

$$MAPE = (100/n)\,\Sigma\left|y_i - \hat{y}_i\right|/y_i\% \tag{3}$$

$$NRMSE = (100/\overline{y})\sqrt{\left((1/n)\Sigma\left(y_i - \hat{y}_i\right)^2\right)}\% \tag{4}$$

where, n is the number of observations, y_i is the observed value, $\hat{y}_i$ is the reference value, and $\overline{y}$ is the mean of observations.

3 Results

As seen in Table 2, the FEM solution for mesh 3 required the shortest runtime, with an electric field MAE lower than 2% relative to the model using the mesh 1. Even though there is an increase in MAE with the reduction in mesh size, the NRMSE for the mesh with the lowest number of elements is lower than 7%. No changes were seen in E for GM, while WM presented a 0.001 and 0.002 V/m reduction in the E magnitude for meshes 2 and 3, respectively.

Figure 5 shows the distribution (on the surfaces) and the average magnitude of electric field for the three meshes of the WM and GM. There was a small variation of E with the mesh resolution, and the average value is higher for WM than GM with the same modulation pattern (oscillatory amplitude).

Figure 6 shows the MAPE and NRMSE along the longitudinal axis of the WM and GM. For the MAPE, it is possible to verify changes of less than 2.5% in WM and 1.5% in GM. For the NRMSE of mesh 2, there is a variation between 2 and 8% in WM but under 1% for GM, while the model with mesh 3 shows a variation between 3 and 14% for WM but below 3% in GM. All these values occur except for the extremity regions (rostral and caudal), which show higher errors due to the greater geometric distortion relative to the mesh 1 caused by local lower resolution.

Table 2. Runtime (single run) to solve the model and electric field data.

Mesh	Time (min)	Tissues	E (V/m)	MAE (V/m)	MAPE (%)	NRMSE (%)
1	51	WM	0.356	–	–	–
		GM	0.254	–	–	–
2	53	WM	0.355	0.002	0.59	2.50
		GM	0.254	0.001	0.29	0.68
3	6	WM	0.354	0.007	1.77	6.21
		GM	0.254	0.003	1.06	2.05

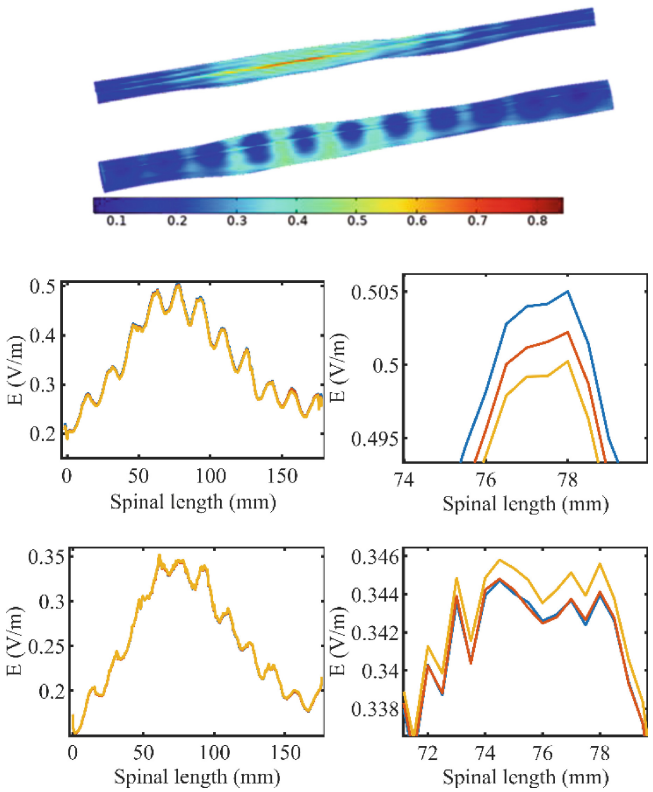

Fig. 5. The magnitude of the electric field distribution on the surfaces of gray matter (first row, top) and white matter. Average magnitude of the electric field across volumetric Sects. (0.5 mm) of the cervical region for the white matter (WM, second row) and gray matter (GM, third row) for three meshes (blue: mesh 1, red: mesh 2, and orange: mesh 3). Electric field zoomed at the C5 vertebra (second column).

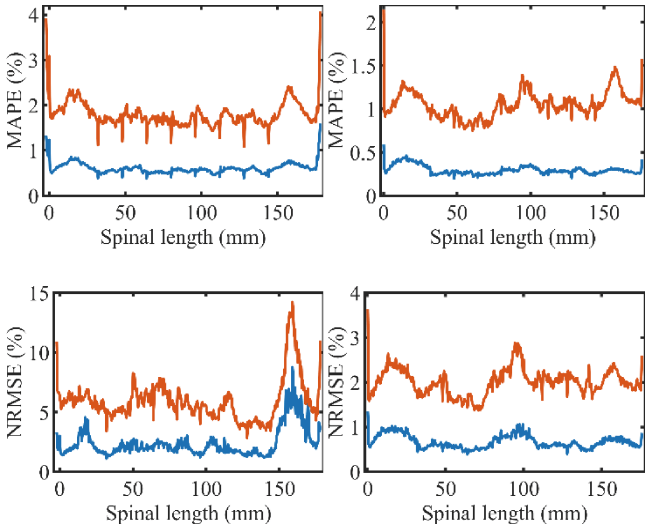

Fig. 6. Electric field error between the simplified meshes and the reference mesh along the cervical region for the white matter (left) and gray matter (right). The blue and red lines show the error for mesh 2 and 3, respectively.

4 Discussion

The goal of our work was to get a simplified model from the cervical region for tsDCS simulations and to implement a low-cost computational simulation by optimizing of the FEM solution with minimal errors in the electric field measured in the target tissues.

We simulated the electric field generated by tsDCS application on the surface of the volume conductor proposed, using three mesh densities for the FEM solution. As the density of the FEM mesh is directly linked to the computational cost necessary for the problem solution, the meshes were built with high, intermediate, and low density. The magnitude of electric field distribution in the meshes of the tissues that form the spinal cord was evaluated and compared. We could not determine any discrepant differences in the average electric field values (Table 2) or in the average electric field distribution between the meshes (Fig. 5). Considering the highest NRMSE, which penalizes larger errors, the overall error was less than 7% (Table 2), while local errors were under 15% (Fig. 6). This can be explained by the quality of the meshes that maintained the Minimum and Average values above 0.02 and 0.65, respectively. Particularly, the Minimum Quality was above 0.1 for the target tissues (WM and GM).

The optimization done in mesh 3 allowed a reduction from 88 to 17 min in processing time (meshing and FEM solution), and from 4 GB to 800 MB (geometry, mesh, and FEM solution) in storage. Additionally, it facilitates variation in parameters such as conductivity, current intensity, and electrode characteristics (e.g., quantity, geometric form, and dimensions) of the tsDCS setup, since any geometric/parametric change requires a new mesh building and solution reprocessing. However, the reduction in the number of elements obtained in mesh 2 did not show the same pattern of reduction in the

processing time of the mesh and the FEM solution. This can happen due to the order of tissue processed and the combination of parameter values used during the mesh 2 setup.

Overall, the electric field distribution shown in Fig. 5 has values in the same range reported by Kuck (max 0.82 V/m) [11] and Fernandes (max 0.5 V/m) [14]. Despite the limitations that the proposed model may present quantitatively in the results, it is believed to provide the necessary information for the intended purpose.

5 Conclusions

It was possible to estimate the electric field in the spinal cord induced by tsDCS using a simplified tissue model of the cervical region. With the parameterization performed during the mesh construction, it was possible to obtain an optimized mesh with a reduced number of elements. The optimized mesh (mesh 3) allowed the runtime for mesh generation to be reduced by three times, and ten times for processing the solution through FEM, while keeping the electric field comparable to the highest resolution one (mesh 1) throughout the entire volume of spinal cord.

Conflict of Interest. The authors declare that they have no conflict of interest.

References

1. Gebodh, N., Esmaeilpour, Z., Adair, D., et al.: Practical Guide to Transcranial Direct Current Stimulation. Springer, Cham (2019)
2. Cogiamanian, F., Ardolino, G., Vergari, M., et al.: Transcutaneous spinal direct current stimulation. Front. Psy. **3**, 63 (2012)
3. Schweizer, L., Meyer-Frießem, C.H., Zahn, P.K., et al.: Transcutaneous spinal direct current stimulation alters resting-state functional connectivity. Brain Connectivity **7**(6), 357–365 (2017)
4. Awosika, O.O., Sandrini, M., Volochayev, R., et al.: Transcutaneous spinal direct current stimulation improves locomotor learning in healthy humans. Brain Stimul. **12**(3), 628–634 (2019)
5. Kaczmarek, D., Ristikankare, J., Jankowska, E.: Does trans-spinal and local DC polarization affect presynaptic inhibition and post-activation depression? J. Physi. **595**(5), 1743–1761 (2017)
6. Grecco, L.H., Li, S., Michel, S., et al.: Transcutaneous spinal stimulation as a therapeutic strategy for spinal cord injury: state of the art. J Neurorestoratology **3**(1), 73–82 (2015)
7. Ahmed, Z.: Trans-spinal direct current stimulation modulates motor cortex-induced muscle contraction in mice. J. Appl. Physiol. **110**(5), 1414–1424 (2011)
8. Bączyk, M., Krutki, P., Zytnicki, D.: Is there hope that transpinal direct current stimulation corrects motoneuron excitability and provides neuroprotection in amyotrophic lateral sclerosis? Physio. Rep. **9**(2), e14706 (2021)
9. Cardoso, J.R.: Electromagnetics through the finite element method: a simplified approach using Maxwell's equations. Crc Press (2016)
10. Dokos, S.: Modelling organs, tissues, cells and devices: using Matlab and Comsol multiphysics. Springer (2017)

11. Kuck, A., Stegeman, D.F., Van Asseldonk, E.H.F.: Modeling trans-spinal direct current stimulation for the modulation of the lumbar spinal motor pathways. J. Neural Eng. **14**(5), 056014 (2017)
12. Fernandes, S.R., Salvador, R., Wenger, C., et al.: Transcutaneous spinal direct current stimulation of the lumbar and sacral spinal cord: a modelling study. J. Neural Eng. **15**(3), 036008 (2018)
13. Dongés, S.C., Bai, S., Taylor, J.L.: Concurrent electrical cervicomedullary stimulation and cervical transcutaneous spinal direct current stimulation result in a stimulus interaction. Exp. Physiol. **102**(10), 1309–1320 (2017)
14. Fernandes, S.R., Pereira, M., Salvador, R., et al.: Cervical trans-spinal direct current stimulation: a modelling-experimental approach. J Neuroeng. Rehabilit. **16**(1), 1–14 (2019)
15. Christ, A., Kainz, W., Hahn, E.G., et al.: The virtual family—development of surface-based anatomical models of two adults and two children for dosimetric simulations. Phys. Med. Biol. **55**(2), N23 (2010)
16. Gosselin, M.C., Neufeld, E., Moser, H. et al.: Development of a new generation of high-resolution anatomical models for medical device evaluation: the virtual population 3.0. Phys. Med. Biol. **59**(18), 5287 (2014)
17. Panjabi, M.M., Duranceau, J., Goel, V. et al.: Cervical human vertebrae. Quantitative three-dimensional anatomy of the middle and lower regions. Spine **16**(8), 861–869 (1991)
18. Panjabi, M.M., Chen, N.C., Shin, E.K., Wang, J.L.: The cortical shell architecture of human cervical vertebral bodies. Spine **26**(22), 2478–2484 (2001)
19. Sengul, G., Watson, C., Tanaka, I., Paxinos, G.: Atlas of the spinal cord: mouse, rat, rhesus, marmoset and human (2013)
20. Frost, B.A., Camarero-Espinosa, S., Foster, E.J.: Materials for the spine: anatomy, problems, and solutions. Materials **12**(2), 253 (2019)
21. Sureka, B., Mittal, M.K., Mittal, A., et al.: Morphometric analysis of diameter and relationship of vertebral artery with respect to transverse foramen in Indian population. Indian J. Rad. Ima. **25**(02), 167–172 (2015)
22. Kwon, S., Suh, S.W., Kim, D., et al.: Analysis of dural sac thickness in the human cervical spine. Anat. Sci. Int. **93**(2), 284–290 (2018)
23. Panjabi, M.M., Oxland, T.R., Parks, E.H.: Quantitative anatomy of cervical spine ligaments. Part II. Middle and lower cervical spine. J. Spinal Dis. **4**(3), 277–285 (1991)
24. Sayit, E., Daubs, M.D., Aghdasi, B., et al.: Dynamic changes of the ligamentum flavum in the cervical spine assessed with kinetic magnetic resonance imaging. Glob. Spi. J. **3**(2), 69–73 (2013)
25. Womack, W., Woldtvedt, D., Puttlitz, C.M.: Lower cervical spine facet cartilage thickness mapping. Osteoarthritis Cartilage **16**(9), 1018–1023 (2008)
26. Schmalfuss, I.M., Mancuso, A.A., Tart, R.P.: Postcricoid region and cervical esophagus: normal appearance at CT and MR imaging. Radiology **214**(1), 237–246 (2000)
27. Furlow, P.W., Mathisen, D.J.: Surgical anatomy of the trachea. Annals of cardiothoracic surgery **7**(2), 255 (2018)
28. Hasgall, P.A. et al.: IT'IS Database for thermal and electromagnetic parameters of biological tissues (2022).https://doi.org/10.13099/VIP21000-04-1
29. Plonsey, R., Heppner, D.B.: Considerations of quasi-stationarity in electrophysiological systems. Bull. Math. Biophys.Biophys. **29**(4), 657–664 (1967)